The Journal of Chemical Physics ARTICLE scitation.org/journal/jcp

Feedback control of protein aggregation

Cite as: J. Chem. Phys. 155, 064102 (2021); doi: 10.1063/5.0055925
Submitted: 4 May 2021 • Accepted: 22 July 2021 •
Published Online: 9 August 2021

Alexander J. Dear,[1] Thomas C. T. Michaels,[1] Tuomas P. J. Knowles,[2] and L. Mahadevan[3,a)]

AFFILIATIONS

[1] School of Engineering and Applied Sciences, Harvard University, Cambridge, Massachusetts 02138, USA
[2] Centre for Misfolding Diseases, Department of Chemistry, University of Cambridge, Lensfield Road, Cambridge CB2 1EW, United Kingdom
[3] School of Engineering and Applied Sciences, Department of Physics, Department of Organismic and Evolutionary Biology, Harvard University, Cambridge, Massachusetts 02138, USA

[a)] **Author to whom correspondence should be addressed:** lmahadev@g.harvard.edu

ABSTRACT

The self-assembly of peptides and proteins into amyloid fibrils plays a causative role in a wide range of increasingly common and currently incurable diseases. The molecular mechanisms underlying this process have recently been discovered, prompting the development of drugs that inhibit specific reaction steps as possible treatments for some of these disorders. A crucial part of treatment design is to determine how much drug to give and when to give it, informed by its efficacy and intrinsic toxicity. Since amyloid formation does not proceed at the same pace in different individuals, it is also important that treatment design is informed by local measurements of the extent of protein aggregation. Here, we use stochastic optimal control theory to determine treatment regimens for inhibitory drugs targeting several key reaction steps in protein aggregation, explicitly taking into account variability in the reaction kinetics. We demonstrate how these regimens may be updated "on the fly" as new measurements of the protein aggregate concentration become available, in principle, enabling treatments to be tailored to the individual. We find that treatment timing, duration, and drug dosage all depend strongly on the particular reaction step being targeted. Moreover, for some kinds of inhibitory drugs, the optimal regimen exhibits high sensitivity to stochastic fluctuations. Feedback controls tailored to the individual may therefore substantially increase the effectiveness of future treatments.

I. INTRODUCTION

Unwanted self-assembly of protein into biofilaments called amyloid fibrils is a core feature of many disease pathologies, including Alzheimer's and Parkinson's diseases,[1–9] sickle-cell anemia,[10,11] type-2 diabetes,[12–14] and the prion diseases.[15–19] Intensive efforts have gone into finding a cure for Alzheimer's in the last two decades.[20] To date, however, although many hundreds of candidate therapies have been developed, almost none have succeeded in clinical trials.[21–24] These failures serve to highlight the need to understand the detailed mechanisms of aggregation into amyloid fibrils and the manner in which the process may be controlled by drugs.

The fundamental kinetic equations describing the formation and growth of biofilaments are by now well-established in the literature.[25–30] Their analytical solution in the past decade[31–34] has permitted the analysis of kinetic data to determine the reaction mechanisms behind formation of different kinds of amyloid.[35–38] This work has paved the way for the design of potential treatments for amyloid diseases that seek to interrupt the aggregation process through inhibition of one or more of the underlying self-assembly reaction steps.[39–46] Crucial to the success of these treatments will be correct dosages and correct timing of administration of the proposed inhibitory drugs, which may be expensive and inherently toxic, as is frequently the case in other diseases, most notably with chemotherapy treatments for cancer.

This task is reminiscent of the classical engineering discipline of optimal control theory, developed in the mid-twentieth century originally to calculate optimal rocket trajectories for the space programs of the USA and USSR.[47] Since then, it has found widespread applications throughout engineering. Given a model for the dynamics and (potentially imprecise) measurements of the system's current state, it formalizes how to guide a dynamical system to a desired outcome by continually updating the values of one or more control variables upon which the dynamics depend. Inspired by a similar analogy, extensive work has been performed in the past 50 years on optimal control of cancer using chemotherapy drugs as control variables, prompted by the high toxicity of most chemotherapy

drugs.[48,49] The use of optimal control theory has also been proposed for the treatment of a variety of other diseases,[50] including HIV[51] and diabetes.[52]

In recent work,[53] we used the theory of optimal control to mathematically determine the most effective times at which to administer drugs for the inhibition of protein filament proliferation in the absence of variation in the dynamics due to, for instance, thermal fluctuations or changes in the availability of nucleation sites. These optimal treatment times were then validated qualitatively against experimental data from a *C. elegans* model of Alzheimer's disease. However, such stochastic fluctuations can exhibit a significant influence on system dynamics,[54,55] and additional measurements of biofilament formation are typically noisy.[56] In this work, we therefore first build on the characterization of optimal drug treatment times in Ref. 53 by calculating the corresponding optimal drug concentrations. We then investigate the extent to which stochastic fluctuations introduce quantitative or qualitative changes in the deterministic optimal control strategies for protein aggregation. This reveals the circumstances under which it may be advantageous to have future drug delivery strategies tailored to individual patients based on feedback from measurements of the progression of the disease in the individual. Such tailored approaches could, in principle, dramatically improve outcomes for patients, particularly if stochastic fluctuations are large.

II. METHODS

We provide in the supplementary material reference tables of all important parameters and functions employed and detailed derivations of key results.

A. Stochastic dynamics of protein filament proliferation in the presence of inhibitory drugs

It has been established that the kinetics of deterministic biofilament formation and growth are well-described by a pair of rate equations for the biofilament number concentration c_a and mass concentration M_a.[25,28–32,57,58] These equations depend on the rate constants for the following fundamental reaction steps for biofilament formation. Primary nucleation occurs with rate constant k_1 and reaction order n_1 with respect to monomers; filament growth through elongation occurs with rate constant k_+. Secondary processes occur with rate constant k_2 and reaction order n_2. The value of this reaction order depends on which secondary process is present: $k_2 \equiv k_-$, $n_2 = 0$ describes filament fragmentation, $n_2 = 1$ corresponds to filament branching, and $n_2 \geq 2$ describes secondary nucleation (Fig. 1).

Here, we restrict our attention to situations in which the monomeric protein concentration c_m is approximately constant, which is likely to be of relevance *in vivo* due to homeostasis and also at earlier reaction times in closed systems *in vitro*. Under such circumstances, it has been shown[32] that after a short initial adjustment period, the protein filament number and mass concentrations become proportional to one another, permitting us to model the proliferation of protein filaments with a single equation,[55]

$$\frac{dc_a}{dt} = \kappa_0 c_a + \frac{\alpha_0}{2}, \tag{1}$$

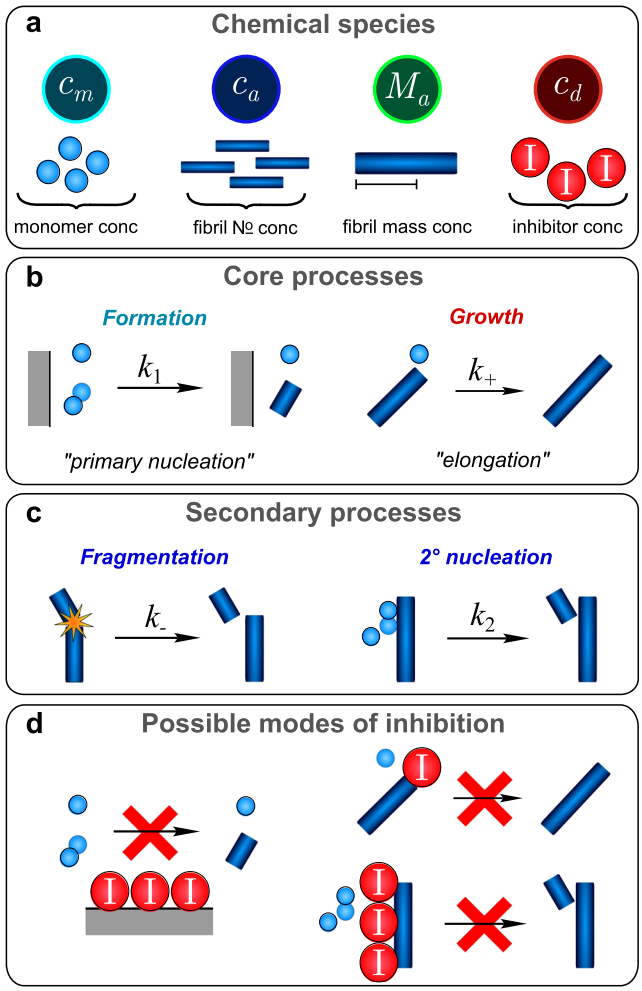

FIG. 1. (a) The fundamental quantities that are required for a dynamical description of the total filament concentration. Note that M_a is not needed when c_m is held constant. (b) Formation of biofilaments always requires the slow formation of new filaments by free association of monomers (primary nucleation), typically at interfaces (gray surface), and the rapid growth of existing filaments by monomer addition. (c) In addition, most systems of biological interest involve a secondary autocatalytic process that generates new biofilaments, such as filament fragmentation, or secondary nucleation of new filaments at the surface of existing filaments. (d) Example modes of action for step-specific inhibition of (clockwise from left) primary nucleation, elongation, and secondary nucleation.

where $\kappa_0 = \sqrt{2k_+k_2c_m^{n_2+1}}$ is the effective proliferation rate and $\alpha_0 = k_1c_m^{n_1}$ is the rate of introduction of new filaments.

Molecular inhibitors may reduce the rate of proliferation of protein filaments by a variety of mechanisms. In all cases, they must bind stoichiometrically to a protein species of interest, which could be in monomeric, oligomeric, or filamentous form, or potentially to an interface in the case of primary nucleation. It has recently been shown[42] that molecular inhibitors, when fast-binding relative to the reaction timescale, can be modeled using a Michaelis–Menten approach, with a steady-state approximation preventing the need to explicitly model bound and free states of protein species.

The dynamics of biofilament proliferation are then still given by Eq. (1) but with modified rates. In Ref. 53, inhibitors were considered that bind monomers (inhibiting every reaction step), fibril surfaces (inhibiting secondary nucleation), fibril ends (inhibiting elongation), or oligomeric intermediates of each nucleation process with equilibrium binding constants $K_m, K_{surf}, K_{ends}, K_{olig,1}$, and $K_{olig,2}$, respectively. In an effort to balance completeness with clarity, we consider here all such inhibitors except those that bind monomers because these likely affect all aggregation reaction steps and their treatment would thus greatly complicate the presentation. We additionally consider inhibitors that bind catalytic surfaces involved in primary nucleation (equilibrium binding constant K_{int}); an *in vitro* example of such a surface is the air–water interface.[59,60] *In vivo*, this inhibition strategy is feasible only when the catalytic surface in question does not perform some critical biological function. Depending on the inhibitor, the resulting modified rate is then one of the following:

$$\alpha(c_d) = \alpha_0\left(\frac{1}{1+K_I c_d}\right), \tag{2a}$$

$$\kappa(c_d) = \kappa_0\left(\frac{1}{1+K_I c_d}\right)^{1/2}, \tag{2b}$$

where c_d is the total drug concentration and K_I is the relevant binding constant [$K_{olig,1}$ or K_{int} in Eq. (2a); K_{surf}, K_{ends}, or $K_{olig,2}$ in Eq. (2b)].

The reaction step that is most likely to be influenced by stochastic effects is thought to be primary nucleation for two key reasons. First, it is highly sensitive to external surfaces and interfaces,[34,60,61] the availability and properties of which are likely to fluctuate significantly in the kind of highly heterogeneous chemical environments found within living organisms. When not too large relative to the nucleation rate, these fluctuations can be reasonably modeled as Gaussian. Second, confinement in volumes (fl–pl) typical of biological environments induces significant stochastic fluctuations in primary nucleation.[62,63] Assuming that the nucleation rate is approximately constant at early times, the stochastic formation of nuclei is naturally governed by a homogeneous Poisson jump process since the number of aggregates is discrete.[55] When the formation rate of nuclei is large enough, however, by the central limit theorem, the Poisson process converges to a Wiener process. Thus, in many cases, stochastic effects can be well-modeled by the introduction of an additive Wiener process to the dynamics, transforming Eq. (1) into a stochastic differential equation (SDE),

$$\frac{dc_a}{dt} = \kappa(c_d)c_a(t) + \frac{\alpha(c_d)}{2} + \sigma_1 \dot{W}_1(t), \tag{3}$$

where $dW_1(t) = \dot{W}_1(t)dt$ is the differential form of a Brownian motion with zero mean and unit variance.

We cannot, in fact, directly access the state c_a experimentally; we instead must take measurements of a phenotype z that depends (preferably linearly) on the state. There are many possible phenotypes; an example in *C. elegans* is the rate of body bends,[43,44,55,64] which is reduced by accumulation of protein aggregates. Another example in humans might be the concentration of a blood-soluble biomarker measured using a diagnostic technique for a neurodegenerative disease.[65] Measurement error is typically well-described as a Gaussian process, in which case the phenotype value z_k measured at time t_k is related to the state as

$$z_k = Hc_a(t_k) + \sigma_2 \dot{W}_2(t_k), \tag{4}$$

where $dW_2(t)$ is the differential form of another Brownian motion with zero mean and unitary variance and zero correlation to $dW_1(t)$. Taken together, Eqs. (3) and (4) define our stochastic dynamical system.

B. Calculating optimal treatment strategies in the absence of stochastic fluctuations

The problem we seek to solve in this paper is how to determine the optimal drug dose regimen for reducing the build-up of toxic protein aggregates in the dynamical system described above, given that drugs may be expensive to obtain and may also have toxic side-effects.

To do so using optimal control theory, a penalty for the deviation of the system from the best possible outcome must first be defined. This penalty, denoted by J, is known as the "cost" and is a functional of the drug regimen. In this paper, we assume that the deviation over a range of times is important, giving rise to a "finite-horizon" cost, which is an integral up to a final time of interest T.[66] For deterministic dynamics, this is

$$J[c_a, c_d] = \int_0^T \mathcal{L}[c_a(t), c_d(t)]dt. \tag{5}$$

One then seeks to minimize the cost functional with respect to the control variable, subject to the constraint that the dynamics of the state variable evolve according to its known rate laws [Eq. (3) with $\sigma_1 = 0$ in the present paper]. [Note that, in other control problems, a "terminal cost" $g(x(T))$ is often added to the cost, where x is the dynamical variable. For simplicity we do not pursue this possibility here.]

The precise form of $\mathcal{L}$ is not yet known for aberrant protein aggregation in biological systems. To capture the essential features of the control problem and to permit its analytical solution, in Ref. 53, the cost function was therefore approximated by the leading-order term in its Taylor expansion $\mathcal{L} = c_a + \zeta c_d$, with ζ being the zeroth order ratio of drug toxicity to aggregate toxicity. Moreover, attention was implicitly restricted to finding optimal "bang–bang" controls for deterministic protein aggregation, in which a constant drug concentration is applied for a finite time period (Fig. 2). The resulting controls have the advantages of being both simple to implement in practice and globally optimal when inhibitor binding is sufficiently unsaturated that the dose–response curve is approximately linear.[66]

Ordinarily, in deterministic optimal control problems, the constrained minimization of Eq. (5) would be achieved by using a continuous analog of a Lagrange multiplier $\lambda(t)$, known as a "costate variable," and then using variational calculus to minimize the following functional with respect to c_a and c_d,

$$\mathcal{F} = J[c_a, c_d] - \int_0^T \lambda(t)\left[\dot{c}_a - \kappa(c_d)c_a - \frac{\alpha(c_d)}{2}\right]dt. \tag{6}$$

Doing so leads to a set of Hamiltonian equations known as the Pontryagin Minimum Principle (PMP).[66] For the linearized cost and

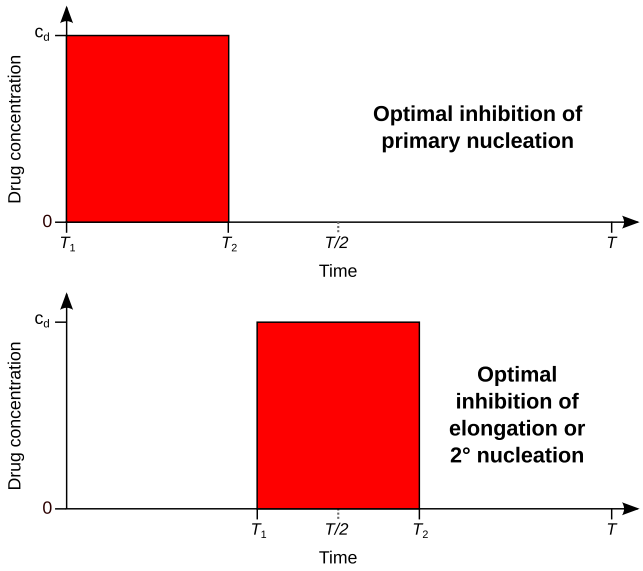

FIG. 2. Optimal bang–bang strategies for the inhibition of deterministic protein aggregation. The drug concentration is zero until the treatment start time T_1, whereupon it is constant at c_d until treatment end time T_2. In Ref. 53, we discovered that inhibitors of primary nucleation must be applied as soon as the aggregation reaction starts. Other inhibitors, on the other hand, must be applied symmetrically about the midpoint of the timespan over which the cost is measured.

bang–bang control discussed above, this yields[53]

$$\mathcal{H} = c_a + \zeta c_d + \lambda(t)\left[\kappa(c_d)c_a + \frac{\alpha(c_d)}{2}\right], \tag{7a}$$

$$\frac{d\lambda(t)}{dt} = -\frac{\partial \mathcal{H}}{\partial c_a} = -1 - \kappa(c_d)\lambda(t), \tag{7b}$$

$$\frac{dc_a(t)}{dt} = \frac{\partial \mathcal{H}}{\partial \lambda} = \kappa(c_d)c_a + \frac{\alpha(c_d)}{2}, \tag{7c}$$

$$0 = \zeta + \lambda(T_i)\left[\kappa' c_a + \frac{\alpha'}{2}\right], \tag{7d}$$

whose solution for $T_i = T_1, T_2$ and for c_d using the terminal (transversality) condition $\lambda(T) = 0$, and appropriate boundary conditions for the aggregation kinetics, leads to the optimal control.[66] The finite differences α' and κ' are defined as

$$\alpha' = \frac{\alpha(c_d) - \alpha_0}{c_d}, \tag{8a}$$

$$\kappa' = \frac{\kappa(c_d) - \kappa_0}{c_d}. \tag{8b}$$

Since $c_d(t)$ is *a priori* specified to be given by a boxcar function, the continuous deformations in c_d upon which variational calculus relies are no longer possible, requiring an alternative derivation for Eq. (7d), which we provide in Appendix A.

The resultant modified PMP was then solved for the optimal bang–bang control start and end times $T_i = T_1, T_2$ for different kinds of inhibition (derivations reproduced in the supplementary material, Sec. II). A key result was that when inhibiting primary nucleation, bang–bang treatment strategies should be started immediately, whereas when inhibiting the other reaction steps, the midpoint of the treatment should be $T/2$ (Fig. 2).

C. Calculating optimal treatments given stochastic dynamics and imperfect measurements

When $\sigma_1 > 0$, our cost becomes a stochastic variable. We must therefore seek to minimize the *expected* cost,

$$J[c_d] = E\left[\int_0^T \mathcal{L}[c_a(t), c_d(t)]dt\right], \tag{9}$$

where $E[\cdots]$ denotes the average over many realizations. Furthermore, we must be prepared to update our control in a feedback manner as T_o increases, and our expectation for the future behavior of the system changes in the light of new data. This is known as a partially observed stochastic control problem, which are frequently encountered in engineering (see Table I for a side-by-side comparison of our problem with a more typical example).

There exists no general approach to solving problems of this kind (see Ref. 67 for a formal treatment). However, for our linearized

TABLE I. Stochastic optimal control in a traditional context (aircraft attitude control) contrasted with stochastic optimal control of protein aggregation.

Dynamical system	Aircraft in flight	Protein aggregation in Alzheimer's disease
		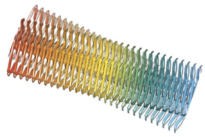
Dynamical variable	Aircraft orientation	Concentration of protein aggregates: c_a
Control variable	Aileron angles	Concentration of inhibitory drug: c_d
Cost function	Deviation from straight-line trajectory	Aggregate and drug toxicity: Eq. (10)
Sources of fluctuations	Turbulence	Confinement effects; nucleation site availability
Measurement techniques	Gyroscopic instruments	Blood tests: $z(t_k)$

$\mathcal{L}$, Eq. (9) can be reduced to the form

$$J[c_d] = E\left[\int_0^T (\hat{c}_a + \zeta c_d)dt\right], \tag{10}$$

where $\hat{c}_a(t)$ is the "filter" for $c_a(t)$ [the best estimate for $c_a(t)$ based on the measurements z_k taken at earlier times $t_k < t$]. Thus, our problem of optimal control of stochastic dynamical systems subject to noisy observations is split into a "filtration" problem and an ordinary stochastic control problem that is fully observed with respect to the filter, an idea known as the *separation principle*.[68] The optimal feedback control c_d is then a function ψ of $\hat{c}_a(t)$, termed a *separated control*, and may be calculated using standard stochastic control techniques. Continuing to focus on a linearized cost thus clearly has the enormous advantage of ensuring that the separation principle applies. This choice of $\mathcal{L}$ is, of course, always accurate for sufficiently small c_a and c_d.

The separation principle only provides useful results if we can compute the filter. However, for nonlinear systems, this is not usually possible. Continuing to optimize only within the space of bang–bang controls therefore has the equally significant advantage of linearizing the stochastic dynamics Eq. (3) and consequently ensuring that the filtration problem admits an analytical solution—the celebrated Kalman filter.[69–72]

By restricting our search to within linear cost functions and bang–bang controls, we can therefore completely solve the problem of stochastic control of protein aggregation with imprecise measurements by first determining the Kalman filter for Eqs. (3) and (4) and then determining the optimal stochastic bang–bang control as a function of this filter but with $\hat{c}_a$ substituted for c_a. These restrictions carry the additional advantage of permitting direct comparison of our results to those of Ref. 53 for deterministic systems.

III. RESULTS

A. Optimal inhibitor dosage for control of protein aggregation

Before considering stochastic protein aggregation, we first compute as a reference the heretofore unknown optimal drug concentrations c_d in the absence of stochastic fluctuations ($\sigma_1 = 0$).

We begin by nondimensionalizing the expressions derived in Ref. 53 for the optimal treatment duration $T_L = T_2 - T_1$ using time units of κ_0^{-1}, a characteristic timescale of protein aggregation [see Eq. (1)], and drug concentration units of K_I^{-1}, where K_I is the equilibrium inhibitor binding constant. We then find that T_L depends only on c_d and on a single dimensionless parameter E, which may be interpreted as the drug efficacy,

$$T_L^{(\alpha)} = T - \ln\left(1 + \frac{1 + c_d}{E}\right), \tag{11}$$

$$T_L^{(\kappa)} \simeq \frac{(1 + c_d)^{1/2}}{(1 + c_d)^{1/2} - 1}\left[T + \ln\left(E\frac{(1 + c_d)^{1/2} - 1}{c_d(1 + c_d)^{1/2}}\right)\right], \tag{12}$$

$$E = \frac{\alpha_0}{2\kappa_0}\frac{K_I}{\zeta}, \tag{13}$$

where the superscript α refers to inhibitors that target solely primary nucleation and κ refers to inhibitors targeting solely another reaction step. Note Eq. (12) is only valid for $e^{T_1^{(\kappa)}} \gg 1$ (see the supplementary material, Sec. II). Taking the limit $c_d \to 0$ reveals that there exist quantifiable E values below which the optimal strategy is always not to treat,

$$E_{\min}^{\alpha} = e^{-T} \quad \text{(for 1° nucleation inhibitors)}, \tag{14}$$

$$E_{\min}^{\kappa} = 2e^{-T} \quad \text{(for all other inhibitors)}. \tag{15}$$

This leads to the interesting observation that the minimum efficacy required to justify the use of drugs targeting primary nucleation is half that required to justify the use of drugs targeting secondary nucleation or elongation.

In Fig. 3, we plot the integrated cost as a function of treatment duration and drug concentration for several values of E; the integrated costs are computed in Appendix B. We see that, especially for small values of E, it may be misleading to identify a single optimal treatment length and drug concentration, as, in fact, a range of treatment parameters give rise to similar overall cost. At higher E values, the optimal strategy is better defined as the cost minimum becomes deeper. Optimal treatments for inhibition of primary nucleation are characterized by a moderate range of possible treatment durations and a wide range of possible drug concentrations. By contrast, optimal treatments for inhibition of primary nucleation are characterized by a wide range of possible treatment durations but a narrow range of possible drug concentrations. Optimal treatment durations for inhibition of primary nucleation are also significantly shorter than those for inhibition of other reaction steps. However, optimal primary nucleation inhibitor concentration is significantly higher than for other types of inhibitor.

Examining Figs. 3(e)–3(h), we see that the globally optimal control strategy for secondary processes features a long treatment time and a low drug concentration for all but the smallest E values. Indeed, the treatment time typically spans almost the whole time interval, rendering Eq. (12) no longer valid at the cost minimum for most values of E, since e^{T_1} is no longer $\gg 1$. To resolve this, we note that for all but the smallest values of E, a treatment strategy with $T_L = T$ exists that has a total cost < 5% greater than the global minimum. Such a strategy is therefore a reasonable approximation of the globally optimal treatment strategy. The corresponding optimal c_d value may be calculated analytically, giving

$$c_d = \left(\frac{T}{2 + W\left[\frac{2(T-E)}{e^2 E}\right]}\right)^2 - 1, \tag{16}$$

where $W[\cdots]$ is the Lambert W-function. In the supplementary material (Sec. III), we illustrate such control strategies and plot Eq. (16).

B. Optimal state estimation with the Kalman filter

In this section, we analyze the Kalman filter and its consequences for measuring protein aggregation.

1. The Kalman–Bucy filter

Given discrete measurements $z_1, \ldots, z_k$, the best estimate $x(t)$ of $c_a(t)$ is provided by the hybrid Kalman filter and can be calculated

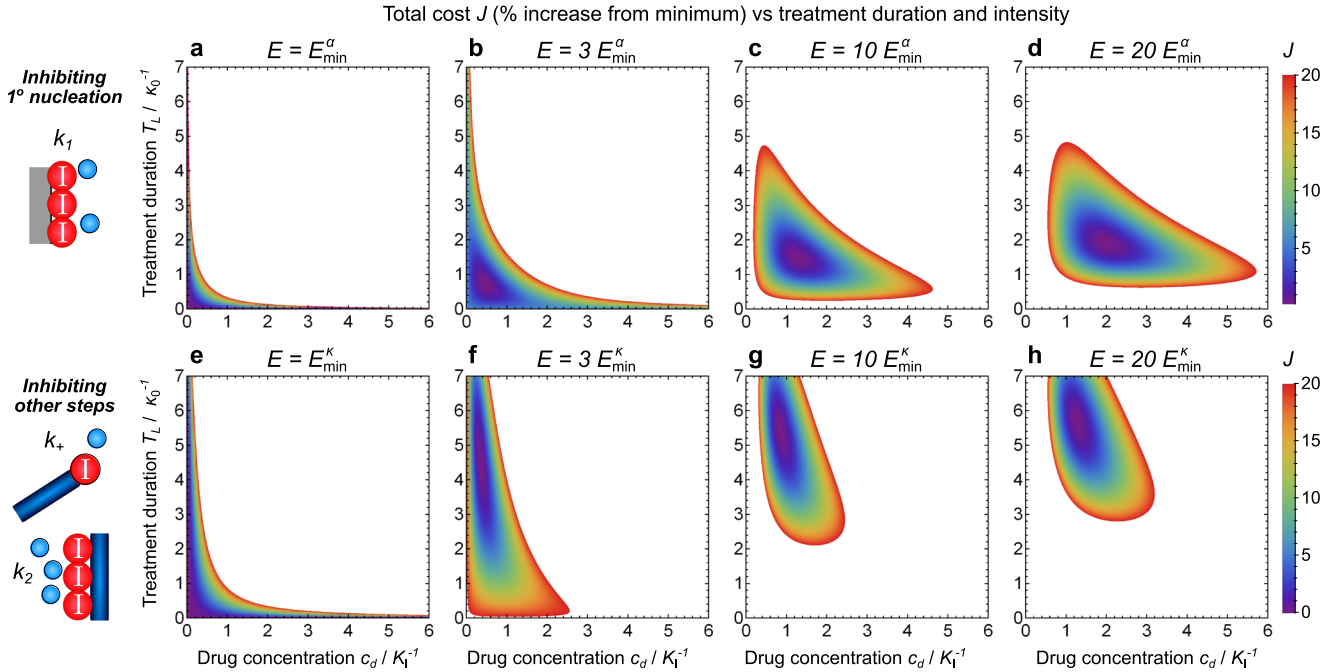

FIG. 3. Total cost J for deterministic protein aggregation subject to a bang–bang regimen for a drug targeting primary nucleation [(a)–(d); Eq. (B2)] or any other step [(e)–(h); Eq. (B4)]. Cost is plotted as a function of drug concentration c_d and treatment length T_L, for several values of $E \geq E_{\min}$, and expressed as % change relative to the global minimum for a given E value. The white regions of the plots correspond to J values above 20%. As E increases, optimal T_L and c_d both increase from zero, as one might expect. However, as $E \to E_{\min}$, almost any T_L value becomes equally effective. Generally, primary nucleation inhibitors should be administered for a short period of time and at a high dose, whereas inhibitors targeting other reaction steps should be used over most of the time period and at relatively lower concentrations. Indeed, for all but the smallest E values, optimal $T_L > T/2$ for the latter inhibitors. There is comparatively greater flexibility in the choice of c_d for primary nucleation inhibitors and in the choice of T_L for other inhibitors. Moreover, while the range of approximately optimal c_d values increases with E, that of T_L values decreases.

algorithmically, given a set of experiments. However, more physical insight can be obtained by considering a continuous-time ansatz $z(t)$ of the data and proceeding analytically. Our phenotype is then related to the state as

$$z(t) = Hc_a(t) + \sigma_2 \dot{W}_2(t). \tag{17}$$

Now, the best estimate $\hat{c}_a(t)$ of $c_a(t)$ is given by the Kalman–Bucy filtering equation,[70]

$$\frac{d\hat{c}_a}{dt} = \kappa(c_d)\hat{c}_a(t) + \frac{\alpha(c_d)}{2} + \mathcal{K}(t)(z(t) - H\hat{c}_a(t)). \tag{18}$$

$\mathcal{K}(t)$, the Kalman gain, is given by a one-dimensional Ricatti Equation (see the supplementary material, Sec. V). If the initial state is precisely known (i.e., zero aggregates) and c_d is constant, then $\mathcal{K}(0) = 0$ and its solution is

$$\mathcal{K}(t,P) = \frac{\kappa}{H}\frac{e^{m\kappa t} - e^{-m\kappa t}}{e^{m\kappa t}/(1+m) - e^{-m\kappa t}/(1-m)}, \tag{19}$$

where

$$m = \sqrt{1 + (1 + K_I c_d)P^2}, \tag{20}$$

$$P = \frac{\sigma_1 H}{\sigma_2 \kappa_0}. \tag{21}$$

P is the relative size of kinetic fluctuations vs measurement noise and can be interpreted as the dimensionless (uninhibited) measurement precision. In this expression, c_d is the concentration of inhibitor of secondary processes or of elongation, not of primary nucleation. We thus see that the inhibited measurement precision is $\sqrt{1 + K_I c_d}P$ and that increasing drug concentration increases the effective measurement precision by increasing the relative size of kinetic fluctuations.

2. Interpreting the value of $\mathcal{K}$

We see from Eq. (18) that the value of $\mathcal{K}$ is essentially the weighting applied to the data measurements relative to the deterministic dynamics when estimating the system state [Fig. 4(a)]. At earlier times, where $\mathcal{K} \simeq 0$, our best guess is the deterministic dynamics, and Eq. (18) simply reduces to the expectation of Eq. (3). This is explained by there being as yet insufficient measurements to significantly update our prior expectation of the dynamical trajectory. Then, $\mathcal{K}$ increases with time, as we accumulate more and more data (i.e., the weight applied to the data correction $z - H\hat{c}_a$ increases). Finally, $\mathcal{K}$ plateaus for large t at a maximum value,

$$\lim_{t\to\infty} \mathcal{K}(t,P) = \frac{\kappa}{H}(1+m), \tag{22}$$

and we stop increasing the weighting of the data correction. It may be shown (see Appendix C) that once this plateau has been reached,

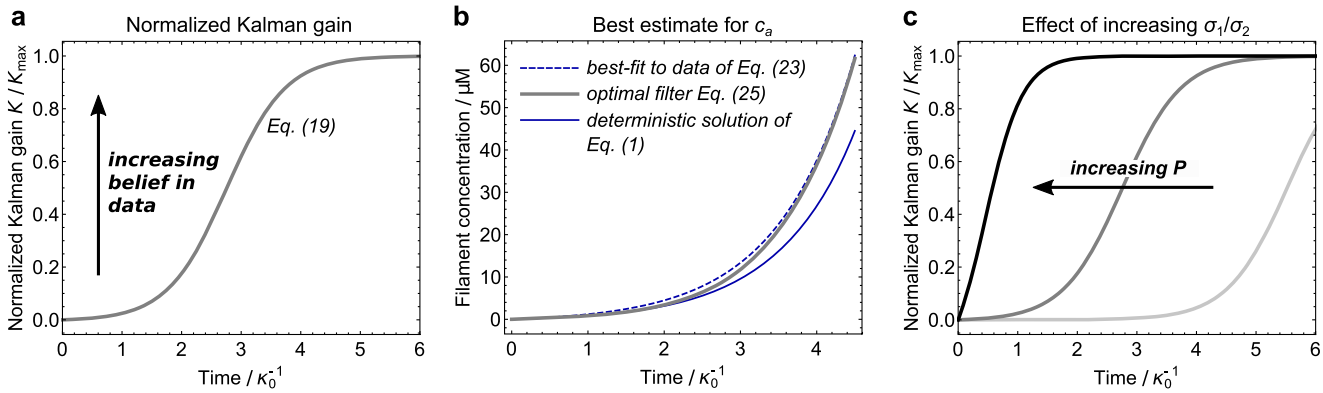

FIG. 4. Illustrating the Kalman gain $\mathcal{K}$. (a) The normalized gain $\hat{\mathcal{K}} = H\mathcal{K}/(\kappa(1+m))$ is interpretable as the % belief in the data relative to the deterministic dynamics. It depends on just two parameters: dimensionless time κt and inhibited measurement precision $\sqrt{1+K_I c_d}P$ [see Eq. (21); set here to 0.125]. $\hat{\mathcal{K}}$ approaches 1 at late times. This reflects that the error of any estimator tends to zero as the number of measurements taken increases. (b) The associated best estimate (gray) for c_a calculated for constant $\tilde{\alpha} = 1.4\alpha$. As expected, the best estimate moves from the deterministic dynamics toward the data ansatz z once the gain starts to significantly increase. (c) $\hat{\mathcal{K}}$ for $P = 0.008$, 0.125, and 1.25; darker gray indicates larger relative measurement precision. Increasing P shifts $\hat{\mathcal{K}}$ toward the origin, as the accuracy of the data as a description of the stochastic dynamics increases relative to that of the deterministic dynamics.

the filter $\hat{c}_a$ becomes equal to the data ansatz $z(t)$,

$$\hat{c}_a(t) \to \frac{z(t)}{H} = \frac{\tilde{\alpha}(T_o)}{2\kappa} e^{\kappa t}, \tag{23}$$

where $\tilde{\alpha}(T_o)$ is determined from fitting the ansatz to the data up to observation time T_o.

3. Interpreting the timing of $\mathcal{K}$

The gain half-time t_h [the time taken for $\mathcal{K}$ to reach half its maximum value Eq. (22)] can be calculated as

$$t_h = \frac{1}{2\kappa m} \ln\left[3 + \frac{2}{m-1}\right]. \tag{24}$$

We see that the half-time decreases with increasing relative measurement precision P [Fig. 4(c)]. This has a clear Bayesian interpretation: our prior for the system dynamics is merely the dynamics with the deterministic nucleation rate. This prior is updated with information from the current experiment (the measurements) until by the plateau value for $\mathcal{K}$ the dynamics estimate is sourced entirely from the data. A larger $P \propto \sigma_1/\sigma_2$ means greater confidence in the new data such that less new data are required before the best estimate of the dynamics ignores the prior expectation for α completely.

4. Best estimate of system state

To solve the system dynamics for general initial conditions $t_0, \hat{c}_a(t_0)$, $\mathcal{K}(t_0)$, we first determine in Appendix C a suitable data ansatz $z(t_e, T_o)$, where the elapsed time $t_e \equiv t - t_0$. We next solve for the Kalman gain with non-zero initial conditions. Substituting these into Eq. (18) permits an analytical solution x for $\hat{c}_a$ (see Sec. VI of the supplementary material for calculation),

$$x(t_e, x_0, c_d, T_o) = \frac{z(t_e, T_o)}{H} + \frac{1+B_0}{e^{m\kappa t_e} + B_0 e^{-m\kappa t_e}}\left[x_0 - \frac{z_0}{H}\right] + \left[\frac{\alpha}{2\kappa} - \frac{\tilde{\alpha}}{2\kappa}\right]\frac{\frac{1}{m}\left(e^{m\kappa t_e} - 1\right) + \frac{B_0}{m}\left(1 - e^{-m\kappa t_e}\right)}{e^{m\kappa t_e} + B_0 e^{-m\kappa t_e}}, \tag{25}$$

where $x_0 = \hat{c}_a(t_e = 0)$, and for simplicity we have chosen elapsed time $t_e - t_0$ as an argument instead of t. Additionally,

$$B_0 = \frac{1 - \hat{\mathcal{K}}(t_0)}{(m-1)/(m+1) + \hat{\mathcal{K}}(t_0)}, \tag{26}$$

where the normalized Kalman gain $\hat{\mathcal{K}} = H\mathcal{K}/(\kappa(1+m))$. The value of B_0 ranges from $(m+1)/(m-1)$ when $\hat{\mathcal{K}}(t_0) \simeq 0$ and the initial state is precisely known to 0 when $\hat{\mathcal{K}}(t_0) \simeq 1$. As expected, as time advances and data continue to accumulate, the deterministic prior for the kinetics no longer matters, and $\hat{c}_a(t) \to z(t - t_0, T_o)/H$ [Fig. 4(b)].

C. Optimal inhibition of primary nucleation

We have already demonstrated that the optimal stochastic controls in the present study are separated controls, of the form $c_d = \psi(\hat{c}_a)$. It can be additionally shown[73] that these controls take the form of the optimal deterministic control expressed in feedback form and with $\hat{c}_a$ substituted for c_a if and only if the previous values of the control have no effect on the variance of c_a conditioned on the data (i.e., when $\Sigma(t) = E\left[\left(c_a(t) - \hat{c}_a(t)\right)^2 | \{z_{i\le k}\}\right]$, where z_k is the most recent measurement and $\{z_{i\le k}\}$ are all the preceding measurements, is independent of past choices of c_d). This property is known as certainty equivalence. For the Kalman filter, $\Sigma(t) = \sigma_2 \mathcal{K}(t)/H$.[70]

The certainty equivalence principle thus holds for drugs targeting solely primary nucleation, since then, $\mathcal{K}(t)$ has no dependence on c_d.

1. Open-loop control

For a linear cost, the optimal deterministic bang–bang control is given by solving Eqs. (7b) and (7d). Since setting $\kappa(c_d) = \kappa_0$ causes c_a to drop out of these equations, we immediately see that the resultant optimal control is open-loop, i.e., with no explicit dependence on the aggregate concentration. It follows that the optimal bang–bang control calculated with a linear cost is entirely unaffected by stochastic fluctuations in the nucleation rate [Figs. 5(a) and 5(b)]. This is less surprising than it may seem since at early times, the Kalman gain is close to zero as we have not collected enough data to prejudice us away from our initial guess for the nucleation rate, α; and, at later times, the current primary nucleation rate no longer affects the dynamics. Thus, at no time do we expect stochastic fluctuations in the rate of primary nucleation to exert a strong influence on the dynamics of the best estimate of the system state.

2. Linear-quadratic-Gaussian control

The immunity of the drug protocol for primary nucleation to stochastic effects given a linear cost is somewhat surprising. To verify the validity of this observation, we note that in the regime that $K_1 c_d \ll 1$, we may linearize the dynamics such that $\alpha(c_d) \simeq \alpha_0 - \alpha_0 K_1 c_d$. If we furthermore switch to a quadratic cost $E[\int_0^T (c_a(t)^2 + (\zeta c_d(t))^2)dt]$, our system reduces to a classical Linear–Quadratic–Gaussian (LQG) problem. Owing to obeying the separation principle, this has a well-known analytical solution which we may use as a benchmark to evaluate the qualitative features of our bang–bang controls. It is given by

$$\frac{d\hat{c}_a}{dt} = \kappa \hat{c}_a(t) + \frac{\alpha_0}{2} - \frac{\alpha_0}{2} K_1 c_d(t) + \mathcal{K}(t)(z(t) - H\hat{c}_a(t)), \quad (27)$$

where α_0 is the uninhibited rate of generation of new filaments and the Kalman gain $\mathcal{K}(t)$ is still given by Eq. (19). The optimal control $c_d(t)$ for inhomogeneous dynamics depends linearly on $\hat{c}_a$ as

$$c_d(t) = \frac{E}{\zeta}(\mathcal{S}(t)\hat{c}_a(t) + \mathcal{R}(t)), \quad (28)$$

where $\mathcal{S}(t)$ is the (nondimensionalized) feedback gain, and $\mathcal{R}(t)$ is the auxiliary gain and are given in Sec. VII of the supplementary material.

In order to obtain $c_d(t)$, we must first solve Eqs. (27) and (28) for $\hat{c}_a(t)$ using an appropriate ansatz $z(t)$ for data collected under the influence of control policy Eq. (28) (computed in Sec. VII of the supplementary material). This yields

$$\hat{c}_a(t) = G(t,T)\int_0^t G^{-1}(s,T)\left(\frac{\alpha_0}{2} + \mathcal{K}(s)z(s) - \kappa E^2 \mathcal{R}(s)\right)ds, \quad (29)$$

where the integrating factor is given by

$$G(t,T) = \frac{(n+1)e^{(n+1)\kappa(t-T)} + (n-1)e^{-(n-1)\kappa(t-T)}}{(1-m)e^{m\kappa t} - (1+m)e^{-m\kappa t}}. \quad (30)$$

This may be solved analytically by noting the numerator of $G \simeq (n+1)e^{(n+1)\kappa(t-T)}$ (see the supplementary material, Sec. VII).

This solution for $\hat{c}_a$ permits us to plot Eq. (28) for $c_d(t)$ in Figs. 5(c) and 5(d). At early times, few aggregates have formed and the control is dominated by $\mathcal{R}(t)$, which depends neither on the data nor on the error, in agreement with the linear cost control. However, at later times, $\hat{c}_a$ gradually begins to depend more strongly on the data and hence the control also does. However, since the control is monotonic decreasing with time, this dependence is very small, even for large P values [Fig. 5(d)].

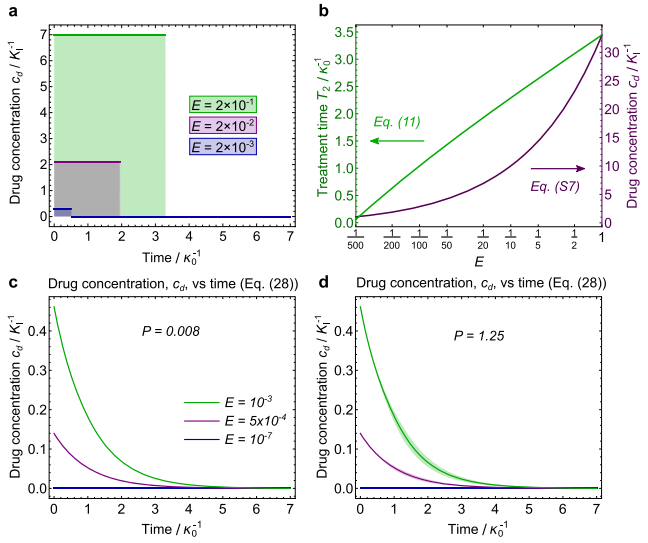

FIG. 5. Optimal control of primary nucleation, using rate constants for Aβ42 aggregation measured *in vitro*,[35] for three different values of drug efficacy $E = \alpha_0 K_1/(2\kappa_0\zeta)$. (a) The optimal bang–bang controls resulting from a linear cost function are unaffected by the introduction of stochastic fluctuations. (b) Optimal c_d rises much more rapidly with E than do treatment times. (c) and (d) Switching to a quadratic cost introduces stochastic variability to the optimal controls. Shading indicates confidence intervals, given large measurement uncertainty $\sigma_2\kappa/H = 0.25\alpha$. (c) The confidence intervals are invisibly small for a value of σ_1 giving low $P = 0.008$. (d) Even for the large stochastic fluctuations, σ_1 needed to give $P > 1$, the confidence intervals for the optimal control policy remain very small. This is in qualitative agreement with the fluctuation-independent bang–bang controls.

D. Optimal inhibition of elongation or of secondary nucleation

For inhibition of secondary nucleation or elongation, κ depends on c_d and thus so does the Kalman filter variance $\Sigma(t) = \sigma_2\mathcal{K}(t)/H$. Thus, given a bang–bang regimen, certainty equivalence does *not* hold. To understand this, consider that it is possible to perturb the control value at any given time away from the certainty equivalent value in a way that reduces the future variance of the filter; this phenomenon is known as *active learning*. A smaller error in the estimated future dynamics translates to a lower expected cost associated with the future control policy. It is moreover possible to choose this perturbation in a way that the decrease in expected cost due to more accurate forecasting outweighs the increase in expected cost due to a suboptimal current control value for the mean dynamics.

1. Approximate separated control strategy

To determine the optimal stochastic control exactly requires numerical methods. Since in this paper we are interested in qualitative analytical results, we instead approximate the optimal control by taking the certainty equivalent control and modifying it to increase its learning potential. Little modification is required at high E, since Fig. 3 shows that small fluctuations in E have little impact on the cost for a given control. An effective modification at low E, on the other hand, is given by increasing c_d by a small amount over the numerically calculated optimal value. This increases the plausible T_1 values dramatically without a concomitant increase in cost. The resultant delayed treatment onset permits sufficient data to be gathered for a relatively accurate choice of T_1 to be made.

2. Determining T_1

To calculate the corresponding optimal certainty equivalent treatment start time for a fixed c_d value requires the straightforward deterministic solution of Eq. (7b) [given by Eq. (S1)] and the setting of $\alpha(c_d) = \alpha_0$ in Eq. (7d), yielding

$$\zeta + \kappa' \hat{c}_a(T_1, T_o)\lambda(T_1) = 0, \tag{31a}$$

$$\zeta + \kappa' \hat{c}_a(T_2, T_o)\lambda(T_2) = 0, \tag{31b}$$

where T_o is again the latest measurement time. For $t \le T_o$, $\hat{c}_a$ is straightforwardly determined from Eq. (25); for $t > T_o$, $\hat{c}_a$ instead evolves according to Eq. (3) with $\sigma_1 = 0$ (see the supplementary material, Sec. VI). Equations (31) are then re-solved numerically for T_1 after each new measurement (performed at time T_o) until T_1 and T_o coincide. Only at this point is the drug administered.

Alternatively, we may develop an approximate approach. If $\mathcal{K}(T_o) \simeq 0$ at $T_o = T_1$, then $\hat{c}_a(t, T_o)$ still equals its deterministic solution and T_1 must take the deterministic value $T_1^{(d)} \simeq T/2 - T_L^{(\kappa)}/2$, expressed in time units of κ_0^{-1} and concentration units of K_I^{-1} as

$$T_1^{(d)} \simeq \frac{T}{2} + \frac{(1+c_d)^{1/2}}{1-(1+c_d)^{1/2}}\left(\frac{T}{2} - \frac{1}{2}\ln\left[\frac{(1+c_d)^{1/2}}{E}\right]\right). \tag{32}$$

On the other hand, when $\mathcal{K}$ has plateaued by T_1, $\hat{c}_a(T_o) \simeq z(T_o, T_o)$. T_1 then takes the limiting value $T_1^{(s)}$, which is $T_1^{(d)}$ but with $\tilde{\alpha}$ substituted for α,

$$T_1^{(s)} \simeq \frac{T}{2} + \frac{(1+c_d)^{1/2}}{1-(1+c_d)^{1/2}}\left(\frac{T}{2} - \frac{1}{2}\ln\left[\frac{(1+c_d)^{1/2}}{E\tilde{\alpha}/\alpha}\right]\right). \tag{33}$$

We expect that T_1 smoothly transitions from $T_1^{(d)}$ to $T_1^{(s)}$ as P increases and the Kalman gain half-time t_h decreases from $> T_1^{(d)}$ to $< T_1^{(s)}$. As such, we expect the value P_{50} of P that gives $t_h = (T_1^{(d)} + T_1^{(s)})/2$ to also correspond to $T_1 = (T_1^{(d)} + T_1^{(s)})/2$. Rather than solving Eq. (31) numerically, this suggests the possibility of using $t_h(P)$, normalized over the range of values of t_h corresponding to $T_1^{(s)} < T_1 < T_1^{(d)}$, as a switching function. Mapping to a Hill function (see Appendix D) gives us the following analytical approximation for T_1:

$$T_1(P) \simeq T_1^{(d)} + S_1(P)\left[T_1^{(s)} - T_1^{(d)}\right], \tag{34a}$$

$$S_1(P) = \frac{P^q}{P_{50}^q + P^q}, \tag{34b}$$

$$P_{50} \simeq 2(1 + K_I c_d)^{-1/2} e^{-(T_1^{(d)} + T_1^{(s)})/2}, \tag{34c}$$

$$q \simeq \frac{4}{T_1^{(d)} - T_1^{(s)} + 2}. \tag{34d}$$

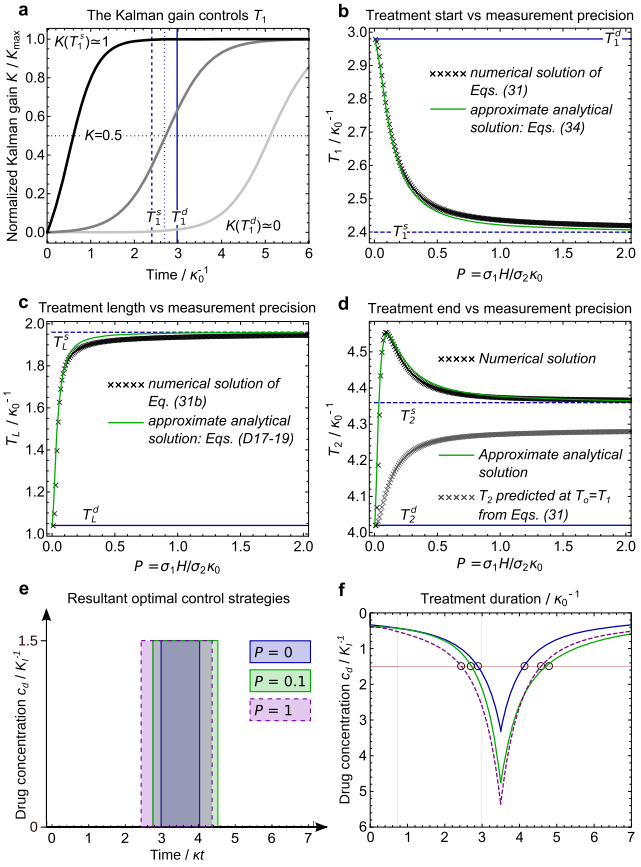

FIG. 6. Dependence of optimal treatment protocols on the scaled measurement precision P (illustrated) for $\tilde{\alpha}(T_2) \simeq \tilde{\alpha}(T_1) = 1.4\alpha$, $E = 3E_{min}^{\kappa}$ and for $K_I c_d = 1.5$. (a) When $P = 0.008$, the normalized Kalman gain $\hat{\mathcal{K}} = H\mathcal{K}/(\kappa(1+m))$ [Eq. (19)] is still small at the deterministic time for treatment onset $T_1^{(d)}$ [Eq. (32)], and we expect $T_1 \simeq T_1^{(d)}$. On the other hand, when $P = 1.25$, $\hat{\mathcal{K}} \simeq 1$ at $t = T_1^{(s)}$ [the treatment onset time calculated from the data alone, Eq. (33)], and we expect $T_1 \simeq T_1^{(s)}$. $P = 0.125$ yields a gain half-time of $T_{50} \equiv (T_1^{(d)} + T_1^{(s)})/2$; we expect this also yields $T_1 = T_{50}$. (b) Numerical simulations confirm these predictions and demonstrate that a switching function in P [Eq. (34)], based on this behavior, gives an accurate approximate analytical solution for T_1. (c) T_L switches from the deterministic value [solid blue line; Eq. (12)] to that calculated using the best-fit kinetics [dashed blue line; Eq. (35)]; a switching function is again a successful approximate solution. (d) T_2 is given from $T_1 + T_L$. It occurs later than predicted at the treatment onset $T_o = T_1$, since $\tilde{\alpha}(T_2)$ is greater than its predicted value, α [see text after Eq. (35) for explanation]. (e) The resulting optimal control strategy for three critical values of P. This is asymmetric for intermediate values of P and clearly very sensitive to stochastic fluctuations. (f) Optimal T_1 and T_2 vs c_d for the same values of P. Increasing c_d reduces treatment duration until the optimal treatment becomes no treatment. By contrast, at low c_d, the optimal treatment is continuous.

This expression is remarkably accurate (Fig. 6), supporting our interpretation of the Kalman gain's role.

3. Determining T_2

The value for T_2 computed above, at $T_o = T_1$, is *not* the optimal time at which to end the control; rather, it is the best guess for T_2, given measurements recorded up to $t = T_1$. The expression for $\hat{c}_a(t, T_o)$ continues to evolve as T_o passes T_1. T_2 is now given by re-solving numerically Eq. (31b) with fixed T_1 after each new measurement until $T_o = T_2$.

Alternatively, for small enough P, the Kalman gain $\mathcal{K}$ remains approximately zero at T_2 and we recover the deterministic value for T_L, Eq. (12). For large enough P, $\mathcal{K}$ has plateaued by T_1 and T_L is instead given in units of κ_0^{-1} by Eq. (12) but with $\bar{\alpha}$ substituted for α,

$$T_L^{(s)} \simeq \frac{(1+c_d)^{1/2}}{(1+c_d)^{1/2}-1}\left(T - \ln\left[\frac{(1+c_d)^{1/2}}{E\bar{\alpha}/\alpha}\right]\right). \tag{35}$$

Once $\mathcal{K}$ plateaus, it becomes apparent to the controller that T_1 and T_2 should have been chosen as $T_1^{(s)}$ and $T_2^{(s)}$. Given the lack of a time dependence to the importance of κ to the dynamics, it is likely more important to retain the correct treatment length than to retain the correct T_2 value. We therefore expect that an approximate analytical solution for T_2 should be developed via a switching function for T_L, not one for T_2 itself, this time considering a P_{50} corresponding to $t_h = (T_2^{(d)} + (T_1^{(d)} + (T_2^{(s)} - T_1^{(s)})))/2$ (see Appendix D for formulas). The accuracy of this approach is demonstrated in Fig. 6, verifying this interpretation. It also leads to the interesting phenomenon that, for a certain range of measurement precisions corresponding to $T_1 < t_h < T_2$, the optimal treatment profile loses its symmetry around $T/2$ as $T_2 \to T_1^{(d)} + T_L^{(s)}$.

IV. CONCLUSIONS

In Sec. III A, we showed that for a given reaction step, the optimal policy depends solely on the dimensionless drug efficacy E [Eq. (13)], interpreted as the ratio of an inhibitor's equilibrium binding constant to its toxicity. Both treatment durations and drug concentrations increase with E. Minimum E values, below which no treatment becomes preferable to treatment, were calculated for each inhibitor target [Eqs. (14) and (15)], revealing that inhibitors of the primary nucleation reaction step can be employed with a lower efficacy than can other inhibitors.

We next showed that the most effective protocols for primary nucleation inhibitors feature short treatment durations but high drug concentrations. Additionally, moderate deviations in both drug concentration c_d and treatment length T_L from the optimum value are relatively well-tolerated. Optimal protocols for inhibitors of the other key reaction steps feature instead lower drug concentrations but much longer treatments, with deviations in T_L (but not c_d) being well-tolerated.

The measurement precision P, defined in Eq. (21) as the nondimensionalized magnitude of stochastic dynamical fluctuations relative to that of the measurement noise, emerges as the key parameter describing stochastic effects. It governs the timescale on which our best guess $\hat{c}_a$ of the kinetic trajectory switches from the deterministic dynamics to the best-fit to the measurements. This switching behavior, explored in Sec. III B, is quantified by the "Kalman gain" $\mathcal{K}(t)$, a sigmoidal function whose control of the filter dynamics is given by Eq. (18). For low values of P, $\mathcal{K}$ remains small for a long time, there is little sensitivity of the filter to measurement fluctuations, and the optimal control remains close to its deterministic analog. At high values of P, $\mathcal{K}$ quickly becomes large, causing the optimal control to potentially deviate from the deterministic control. This behavior can be rationalized by considering that at low P values, we have little faith in the accuracy of our measurements, so reverting to the deterministic control is the best course of action. At higher P, our measurements instead provide a good estimate of the kinetics after only a few measurements have been taken. In this regime, when significant stochastic fluctuations occur, they are quickly detected and the optimal control is updated in response.

We showed in Sec. III C that optimal drug treatment regimens for inhibitors of primary nucleation are certainty equivalent, meaning they are identical to deterministic regimens but with their feedback dependence on c_a replaced by a dependence on $\hat{c}_a$. We also found that optimal drug treatment regimens for such inhibitors are only weakly affected by stochastic fluctuations. By contrast, we demonstrated in Sec. III D that optimal treatment regimens for other kinds of inhibitors exhibit delayed onset compared to the certainty equivalent regimen. By permitting more data to accumulate prior to treatment onset, this enables a more accurate choice of the regimen to be made. These treatments are moreover heavily influenced by stochastic fluctuations. Tailoring regimens to specific patients is thus much more important for inhibitors of secondary nucleation and of elongation than for primary nucleation inhibitors, particularly at lower values of E, where treatment can be delayed without significant cost penalty while further data are gathered.

We have restricted our attention to the boxcar drug concentration functions shown in Fig. 2 to aid comparison with previous work and to permit analytical solutions to the equations governing optimal treatments. We leave to future studies the analysis of more flexible and realistic treatment protocols that explicitly account for drug metabolism and finite absorption rates, which will require avery different (numerical) methodology. However, typical timescales for drug absorption and degradation are short compared to typical treatment durations, so we expect the conclusions drawn in the present work to remain broadly valid.

Our approach in this paper has assumed perfect knowledge of the bulk rate constants of protein aggregation. In reality, these are expected to vary between individuals and are thus not known *a priori*; they must instead be computed on the fly. At least three independent fields have arisen within engineering that, based on different assumptions, seek optimal controls for systems with imperfectly known models: robust control, model predictive control, and adaptive control. A valuable next step would be to adapt methodologies from these fields to account for rate constant uncertainty when designing optimal stochastic treatment regimens.

SUPPLEMENTARY MATERIAL

See the supplementary material for the summary of parameters used in this paper and for detailed derivations of various key mathematical results.

ACKNOWLEDGMENTS

We acknowledge support from the Lindemann Trust Fellowship, English-Speaking Union (A.J.D.); the Swiss National Science Foundation (T.C.T.M.); Peterhouse, Cambridge (T.C.T.M.); the Frances and Augustus Newman Foundation (T.P.J.K.); the NSF-Simons CMSAB 1764269, the MacArthur Foundation and the Henri Seydoux Fund (L.M.).

APPENDIX A: PROVING THE FINITE DIFFERENCE FORMULAS

Here, given its importance, we confirm the validity of Eq. (7d) by providing an explicit derivation. If we write $c_d(t)$ explicitly as a boxcar function with start and end times T_1 and T_2 and fixed drug concentration between these times of c_d, Eq. (6) reduces to

$$\begin{aligned}\mathcal{F} = &\int_0^{T_1}\left[c_a(t) - \lambda(t)\left(\dot{c}_a - \kappa_0 c_a(t) - \frac{\alpha_0}{2}\right)\right]dt \\ &+ \int_{T_1}^{T_2}\left[c_a(t) + \zeta c_d - \lambda(t)\left(\dot{c}_a - \kappa(c_d)c_a(t) - \frac{\alpha(c_d)}{2}\right)\right]dt \\ &+ \int_{T_2}^{T}\left[c_a(t) - \lambda(t)\left(\dot{c}_a - \kappa_0 c_a(t) - \frac{\alpha_0}{2}\right)\right]dt. \end{aligned} \tag{A1}$$

For a fixed c_d, we then compute the derivatives with respect to the variables T_1 and T_2 using Leibniz' rule. Using Eqs. (8b) and (8a), this yields

$$\frac{d\mathcal{F}}{dT_1} = -\zeta c_d - \kappa' c_a(T_1)\lambda(T_1)c_d - \frac{\alpha'}{2}\lambda(T_1)c_d, \tag{A2}$$

$$\frac{d\mathcal{F}}{dT_2} = \zeta c_d + \kappa' c_a(T_2)\lambda(T_2)c_d + \frac{\alpha'}{2}\lambda(T_2)c_d. \tag{A3}$$

Minimizing the cost $\mathcal{F}$ by setting these derivatives to zero then recovers Eq. (7d) and demonstrates that it is solved at times T_1 and T_2.

APPENDIX B: COST FUNCTIONS FOR BANG–BANG CONTROL OF DETERMINISTIC PROTEIN AGGREGATION

We present here the integrated costs for bang–bang control strategies for deterministic protein aggregation.

1. Inhibition of primary nucleation

Writing $\varepsilon = \alpha_0/2\kappa_0$, we may explicitly write the cost function in integrated form as

$$\text{Cost} = \int_0^{T_2}[\zeta c_d + c_a(t)]dt + \int_{T_2}^{T} c_a(t)dt.$$

Integrating and nondimensionalizing, we yield

$$\begin{aligned}\frac{\kappa_0}{\varepsilon}\text{Cost} &= \frac{\zeta c_d T_2}{K_{1\varepsilon}} + \frac{\alpha_0}{1+c_d}\left(e^{T_2}-1\right) + \frac{\alpha_0}{1+c_d}\left(e^{T_2}-1\right)\left[e^{T-T_2}-1\right] \\ &\quad + \left[e^{T-T_2}-1\right] - (T-T_2) - \frac{\alpha_0}{1+c_d}T_2 \\ &= \frac{c_d T_2}{E} + \frac{\alpha_0}{1+c_d}\left(e^{T_2}-1\right)e^{T-T_2} \\ &\quad + \left[e^{T-T_2}-1\right] - T + T_2\left(1 - \frac{\alpha_0}{1+c_d}\right). \end{aligned} \tag{B1}$$

Realizing that the terms linear in T_2 from the aggregate cost are comparatively unimportant (and of uncertain validity due to the approximate nature of the nonexponential term in c_a) and dropping constant terms, we finally have

$$T + 1 + \frac{\kappa_0}{\varepsilon}\text{Cost} \simeq \frac{c_d T_2}{E} + \frac{\alpha_0}{1+c_d}e^{T} + \left(1 - \frac{\alpha_0}{1+c_d}\right)e^{T-T_2}. \tag{B2}$$

This is exactly Eq. (S102) from Ref. 53 and is plotted in Fig. 3. The optimal c_d may either be computed by finding the minimum numerically or an approximation may be developed (see the supplementary material, Sec. III).

2. Inhibition of elongation or secondary nucleation

Recalling the deterministic solutions for c_a, Eq. (S71) from Ref. 53,

$$c_a(T_1) = \begin{cases} \varepsilon\left(e^{\kappa_0 t} - 1\right), & t \le T_1, \\ c_a(T_1)e^{\kappa(t-T_1)} + \dfrac{\varepsilon\kappa_0}{\kappa}\left(e^{\kappa(t-T_1)} - 1\right), & T_1 < t \le T_2, \\ c_a(T_2)e^{\kappa_0(t-T_2)} + \varepsilon\left(e^{\kappa_0(t-T_2)} - 1\right), & t > T_2, \end{cases} \tag{B3}$$

the cost integral becomes

$$\begin{aligned}\text{Cost} &= \int_0^{T_1} c_a(t)dt + \int_{T_1}^{T_2}[\zeta c_d + c_a(t)]dt + \int_{T_2}^{T} c_a(t)dt \\ &= \zeta c_d T_L + \frac{\varepsilon}{\kappa_0}\left(e^{\kappa_0 T_1} - \kappa_0 T_1 - 1\right) + \frac{c_a(T_1)}{\kappa}\left[e^{\kappa T_L} - 1\right] \\ &\quad + \frac{\varepsilon\kappa_0}{\kappa^2}\left[e^{\kappa T_L} - \kappa T_L - 1\right] + \frac{c_a(T_2)}{\kappa_0}\left[e^{\kappa_0(T-T_2)} - 1\right] \\ &\quad + \frac{\varepsilon}{\kappa_0}\left[e^{\kappa_0(T-T_2)} - \kappa_0(T-T_2) - 1\right]. \end{aligned}$$

Nondimensionalizing and writing $\kappa_I = \kappa/\kappa_0$, we get

$$\begin{aligned}\frac{\kappa_0}{\varepsilon}\text{Cost} &= \frac{T_L c_d}{E} + T_L\left(1 - \frac{1}{\kappa_I}\right) - T + 2\frac{c_a(T_1)}{\varepsilon} + 2\frac{c_a(T_1)}{\varepsilon\kappa_I}\left[e^{\kappa_I T_L} - 1\right] \\ &\quad + \frac{1}{\kappa_I^2}\left[e^{\kappa_I T_L} - 1\right] + \frac{c_a(T_1)^2}{\varepsilon^2}e^{\kappa_I T_L}. \end{aligned} \tag{B4}$$

This is plotted in Fig. 3. To obtain the optimal c_d, we must find the minimum numerically. Note the cost function contains several important terms in addition to those in Eq. (S103) from Ref. 53, which have a large qualitative effect on the solution for c_d. In Sec. III of the supplementary material, we instead pursue an approximate solution for the optimal c_d.

APPENDIX C: DETERMINING THE ANSATZ $z(t)$ FOR CONSTANT c_d

For Wiener input, the stochastic time evolution of the polymer mass concentration $c_a(t)$ is given by the following SDE:

$$dc_a(t) = \left[\kappa c_a(t) + \frac{\alpha}{2}\right]dt + \sigma_1 dW(t), \tag{C1}$$

where $dW(t)$ is the differential form of a Brownian motion with zero mean and unitary variance. The quantity $\alpha/2$ in Eq. (C1) represents the deterministic part of the aggregate input through primary nucleation, whereas the parameter σ_1 measures the amplitude of the variation of the primary nucleation rate.

Since σ_1 is constant, either Ito or Stratonovich calculus can equally be used, regardless of the physical origin of the noise term.[74] Using Stratonovich calculus permits a straightforward integration to give

$$c_a(t) = c_a(0)e^{\kappa t} + \frac{\alpha}{2\kappa}(e^{\kappa t} - 1) + \sigma_1 \int_0^t e^{\kappa(t-s)} dW(s). \tag{C2}$$

The first two terms on the right-hand side of Eq. (C2) describe the deterministic dynamics, while the last term describes the stochastic part in the form of a convolution of the instantaneous noise input $dW(s)$ and the exponential propagation term $e^{\kappa(t-s)}$.

1. Equivalence of Wiener process noise to stochastic initial α choice

When $e^{\kappa t} \gg 1$, which is the limit that we care about, as this is the limit in which our SDEs are correct, we may write

$$c_a(t) = \left(c_a(0) + \frac{\alpha}{2\kappa} + \sigma_1 \int_0^t e^{-\kappa s} dW(s)\right) e^{\kappa t}. \tag{C3}$$

The integral J may be written as

$$J = \int_0^\infty e^{-\kappa s} dW(s) - \int_t^\infty e^{-\kappa s} dW(s).$$

Since $e^{-\kappa s} \ll 1, \quad t < s < \infty,$

$$J \simeq \int_0^\infty e^{-\kappa s} dW(s) = \text{constant}$$

and

$$c_a(t) \simeq \frac{\alpha_f}{2\kappa} e^{\kappa t} + c_a(0)e^{\kappa t}, \tag{C4}$$

where

$$\alpha_f = \alpha + 2\sigma \int_0^\infty \kappa e^{-\kappa s} dW(s). \tag{C5}$$

To a good approximation, therefore, we expect that the stochastic progress curve can be represented by a deterministic curve with deterministic κ and a stochastic effective nucleation rate α_f, whose value becomes apparent once $t \gtrsim \kappa^{-1}$.

2. z ansatz

With measurement error, α_f is not precisely known even in this limit; it may instead be estimated by least-squares fitting of Eq. (C4), with the fitting parameter α_f to the data. Thus, when $c_a(0) = 0$, the most appropriate choice of ansatz for z is

$$z(t) = H\frac{\bar{\alpha}(T_o)}{2\kappa} e^{\kappa t}, \tag{C6}$$

where $\bar{\alpha}(T_o)$ is the best fit value for the effective nucleation rate α_f obtained by fitting z to data collected up to observation time T_o and where $t \le T_o$. In the seeded case, this clearly generalizes to

$$z(t, t_0, T_o) = (H\bar{\alpha}/(2\kappa))(e^{\kappa(t-t_0)} - 1) + z_0(T_o)e^{\kappa(t-t_0)}, \tag{C7}$$

fitting z_0 from the available data.

3. The ansatz is recovered when $\mathcal{K}$ plateaus

In the plateau region, $\mathcal{K}$ is constant at $(1+m)\kappa/H$, and z is the exponential function Eq. (C6). Now, feeding these into the Kalman filtering equation (18),

$$\frac{d\hat{c}_a}{dt} + m\kappa\hat{c}_a = \frac{\alpha}{2} + \frac{\bar{\alpha}(T_o)}{2}(1+m)e^{\kappa t}. \tag{C8}$$

In the plateau region, $e^{\kappa t} \gg 1$, so we may neglect the first term of the RHS. Integrating yields

$$\hat{c}_a(t) = \hat{c}_a(t_0)e^{-m\kappa(t-t_0)} + e^{-m\kappa t}\int_{t_0}^t \frac{\bar{\alpha}(T_o)}{2}(1+m)e^{(1+m)\kappa s} ds. \tag{C9}$$

Once more we may neglect the first term once we are well into the plateau, whereupon we recover

$$\hat{c}_a(t) = \frac{\bar{\alpha}(T_o)}{2\kappa} e^{\kappa t}; \tag{C10}$$

in other words, the filter becomes equal to the data ansatz once enough time has elapsed that we have entered the plateau region of the Kalman gain.

APPENDIX D: SWITCHING FUNCTIONS

To determine approximate expressions for how T_1 and T_2 change with P, we must first investigate how the gain half-time depends on P. Equation (24) for the gain half-time is not precisely invertible for P; however, restricting our attention to half-times greater than the adjustment time, i.e., $e^{2\kappa t_h} \gg 1$, Eq. (24) is only satisfied for $m \to 1$. In this limit, Eq. (24) reduces to

$$e^{2m\kappa t_h} \simeq \frac{2}{m-1}. \tag{D1}$$

This is solved by

$$m_h(t_h) = 1 + \frac{1}{2\kappa t_h} W\left[4\kappa t_h e^{-2\kappa t_h}\right], \tag{D2}$$

$$\simeq 1 + 2e^{-2\kappa t_h}, \tag{D3}$$

where the second line follows since the argument of the Lambert W-function $W[\cdots]$ is small. In the limit $m \to 1$, $m \simeq 1 + (1 + K_I c_d)P^2/2$, and thus,

$$P_h(t_h) \simeq 2(1 + K_I c_d)^{-1/2} e^{-\kappa t_h}, \tag{D4}$$

$$t_h(P_h) \simeq \frac{1}{\kappa} \ln\left[\frac{2}{\sqrt{1 + K_I c_d} P_h}\right], \tag{D5}$$

$$\frac{dt_h}{dP_h} \simeq -\frac{1}{\kappa P_h}, \tag{D6}$$

where $\{m_h, P_h\}(t_h)$ are the values of m or P required to yield a particular half-time t_h.

It is also of interest to consider the gradient of $\hat{\mathcal{K}}$ at half maximum, which we will later use to estimate the width of the gain sigmoidal,

$$\frac{1}{\kappa}\frac{d\hat{\mathcal{K}}}{dt} = \frac{me^{m\kappa t} + me^{-m\kappa t}}{e^{m\kappa t} - \frac{1+m}{1-m}e^{-m\kappa t}} - \hat{\mathcal{K}}\frac{me^{m\kappa t} + m\frac{1+m}{1-m}e^{-m\kappa t}}{e^{m\kappa t} - \frac{1+m}{1-m}e^{-m\kappa t}}$$

$$\Rightarrow \left.\frac{d\hat{\mathcal{K}}}{dt}\right|_{t=t_h} = \frac{\kappa}{2}\frac{me^{2m\kappa t_h} + m\left(2 - \frac{1+m}{1-m}\right)}{e^{2m\kappa t_h} - \frac{1+m}{1-m}}$$

$$= \frac{\kappa}{2}\frac{m\frac{1-3m}{1-m} + m\frac{1-3m}{1-m}}{\frac{1-3m}{1-m} - \frac{1+m}{1-m}} = m\kappa\frac{1-3m}{1-3m-(1+m)}$$

$$\therefore \left.\frac{d\hat{\mathcal{K}}}{dt}\right|_{t=t_h} = \kappa\frac{3m_h - 1}{4} \simeq \frac{\kappa}{2} + \frac{3\kappa}{8}(1 + K_I c_d)P_h^2. \tag{D7}$$

1. Switching function for T_1

The point at which $\mathcal{K}$ gives $T_1 = T_{50} = (T_1^{(d)} + T_1^{(s)})/2$ is when $t_h \simeq T_{50}$. Since initially $c_d = 0$, the corresponding P_h value is

$$P_{50} = 2e^{-\kappa_0 T_{50}}. \tag{D8}$$

We must consider now the range of values of t_h corresponding to the range of values of T_1 from $T_1^{(d)}$ to $T_1^{(s)}$. This is from $T_1^{(s)} - w/2$ to $T_1^{(d)} + w/2$, where w is the width of the sigmoidal in units of κ_0^{-1}. This can be estimated by approximating $d\hat{\mathcal{K}}/dt$ as a boxcar function with the top being equal to the gradient at half maximum. The width is then approximately

$$w \simeq \left.\frac{dt}{d\hat{\mathcal{K}}}\right|_{t=t_h} \simeq \frac{1}{\kappa_0}\frac{8}{4 + 3P_{50}^2}. \tag{D9}$$

The range for normalization is then

$$N = T_1^{(d)} - T_1^{(s)} + w \simeq T_1^{(d)} - T_1^{(s)} + \frac{1}{\kappa_0}\frac{8}{4 + 3P_{50}^2}. \tag{D10}$$

The normalized gradient at half maximum is thus

$$\frac{1}{N}\left.\frac{dt_h}{dP}\right|_{P=P_{50}} = -\frac{1}{\kappa_0 N P_{50}}. \tag{D11}$$

The Hill function has form $S_1(P) = P^q/(P_{50}^q + P^q)$. The gradient at half maximum is

$$\frac{dS_1}{dP} = \frac{q}{P}S_1(P) - \frac{q}{P}S_1(P)^2, \tag{D12}$$

$$\therefore \left.\frac{dS_1}{dP}\right|_{P=P_{50}} = \frac{q}{4P_{50}}. \tag{D13}$$

Matching absolute gradients, we have

$$q = \frac{4}{\kappa_0 N} = \left(\frac{\kappa_0(T_1^{(d)} - T_1^{(s)})}{4} + \frac{2}{4 + 3P_{50}^2}\right)^{-1}$$

$$= \left(\frac{\kappa_0(T_1^{(d)} - T_1^{(s)})}{4} + \frac{1}{2 + 6e^{-\kappa_0(T_1^{(d)} + T_1^{(s)})}}\right)^{-1}$$

$$\simeq \frac{4}{\kappa_0(T_1^{(d)} - T_1^{(s)}) + 2}. \tag{D14}$$

The switching function described by Eq. (34) follows.

2. Switching function for T_L

We now turn our attention to developing a switching function for the treatment length T_L. The lengths to be interpolated between are $T_L^{(d)} = T_2^{(d)} - T_1^{(d)}$ and $T_L^{(s)} = T_2^{(s)} - T_1^{(s)}$; the corresponding times to be interpolated between are $T_2^{(d)}$ and $T_1^{(d)} + T_L^{(s)}$. Our switching half-time is then $t_h \simeq T_{50,L} = (T_2^{(d)} + T_1^{(d)} + T_L^{(s)})/2$.

The drug concentration changes before T_2 is reached, so, in principle, we should use the seeded Kalman gain Eq. (S25) to calculate the P value giving this switching half-time. However, this does not give rise to a simple analytical solution for P, so we instead calculate two P values using the unseeded Eq. (24) as before: one for $c_d = 0$ and one for $c_d \neq 0$. We then take the average of these values weighted by the approximate proportion of time the system spends in each drug concentration state before $t = T_2$. The inhibited and uninhibited values, respectively, are found to be

$$P_{50,L(i)} = 2(1 + K_I c_d)^{-1/2} e^{-\kappa T_{50,L}}, \tag{D15}$$

$$P_{50,L(u)} = 2e^{-\kappa_0 T_{50,L}}. \tag{D16}$$

Our averaged value is then

$$P_{50,L} = \frac{P_{50,L(u)}(T_1^{(d)} + T_1^{(s)}) + P_{50,L(i)}(T_L^{(d)} + T_L^{(s)})}{T_1^{(d)} + T_1^{(s)} + T_L^{(d)} + T_L^{(s)}}. \tag{D17}$$

We take a different approach for computing the exponent. This essentially depends on the slope of the seeded Kalman gain around its half-time, which can be reasonably approximated by the slope of the unseeded Kalman gain with drug concentration c_d around its own half-time. The time range to normalize over is thus

$$N_L = T_1^{(d)} + T_L^{(s)} - T_2^{(d)} + w(i)$$

$$\simeq T_L^{(s)} - T_L^{(d)} + \frac{1}{\kappa}\frac{8}{4 + 3(1 + K_I c_d)P_{50,L(i)}^2}. \tag{D18}$$

Matching the normalized gradient of the gain half-time at half maximum to that for a Hill function with order q_L gives

$$q_L = \frac{4}{\kappa N_L} = \left(\kappa\frac{T_L^{(s)} - T_L^{(d)}}{4} + \frac{2}{4 + 3(1 + K_I c_d)P_{50,L(i)}^2}\right)^{-1}$$

$$= \left(\kappa\frac{T_L^{(s)} - T_L^{(d)}}{4} + \frac{1}{2 + 6e^{-(T_2^{(d)} + T_1^{(d)} + T_L^{(s)})}}\right)^{-1}$$

$$\simeq \frac{4}{\kappa(T_L^{(s)} - T_L^{(d)}) + 2}. \tag{D19}$$

$P_{50,L}$ and q_L together define the Hill switching function for T_L.

DATA AVAILABILITY

Data sharing is not applicable to this article as no new data were created or analyzed in this study.

REFERENCES

[1] C. M. Dobson, Trends Biochem. Sci. **24**, 329 (1999).
[2] F. Chiti and C. M. Dobson, Annu. Rev. Biochem. **75**, 333 (2006).
[3] C. M. Dobson, Nature **426**, 884 (2003).
[4] F. E. Cohen and J. W. Kelly, Nature **426**, 905 (2003).
[5] D. J. Selkoe, Nature **426**, 900 (2003).
[6] P. T. Lansbury and H. A. Lashuel, Nature **443**, 774 (2006).
[7] M. B. Pepys, Philos. Trans. R. Soc., B **356**, 203 (2001).
[8] J. Hardy and D. J. Selkoe, Science **297**, 353 (2002).
[9] J. C. Sacchettini and J. W. Kelly, Nat. Rev. Drug Discovery **1**, 267 (2002).
[10] J. Hofrichter, P. D. Ross, and W. A. Eaton, Proc. Natl. Acad. Sci. U. S. A. **71**, 4864 (1974).
[11] M. Coletta, J. Hofrichter, F. A. Ferrone, and W. A. Eaton, Nature **300**, 194 (1982).
[12] S. B. Padrick and A. D. Miranker, Biochemistry **41**, 4694 (2002).
[13] J. D. Green, C. Goldsbury, J. Kistler, G. J. S. Cooper, and U. Aebi, J. Biol. Chem. **279**, 12206 (2004).
[14] L. Haataja, T. Gurlo, C. J. Huang, and P. C. Butler, Endocr. Rev. **29**, 303 (2008).
[15] S. Prusiner, Science **252**, 1515 (1991).
[16] J. H. Come, P. E. Fraser, and P. T. Lansbury, Proc. Natl. Acad. Sci. U. S. A. **90**, 5959 (1993).
[17] A. Aguzzi and C. Haass, Science **302**, 814 (2003).
[18] J. Falsig, K. P. R. Nilsson, T. P. J. Knowles, and A. Aguzzi, HFSP J. **2**, 332 (2008).
[19] A. Aguzzi and T. O'Connor, Nat. Rev. Drug Discovery **9**, 237 (2010).
[20] J. L. Cummings, T. Morstorf, and K. Zhong, Alzheimer's Res. Ther. **6**, 37 (2014).
[21] Alzheimer's Association, Treatments for Alzheimer's and Dementia, 2020, https://www.alz.org/alzheimers-dementia/treatments.
[22] F. Panza, M. Lozupone, G. Logroscino, and B. P. Imbimbo, Nat. Rev. Neurol. **15**, 73 (2019).
[23] S. Linse, Pure Appl. Chem. **91**, 211 (2019).
[24] S. Linse, T. Scheidt, K. Bernfur, M. Vendruscolo, C. M. Dobson, S. I. A. Cohen, E. Sileikis, M. Lundquist, F. Qian, T. O'Malley, T. Bussiere, P. H. Weinreb, C. K. Xu, G. Meisl, S. Devenish, T. P. J. Knowles, and O. Hansson, Nat Struct Mol Biol **27**, 1125–1133 (2020).
[25] F. Oosawa and M. Kasai, J. Mol. Biol. **4**, 10 (1962).
[26] F. Oosawa and S. Asakura, *Thermodynamics of the Polymerization of Protein* (Academic Press, 1975).
[27] M. F. Bishop and F. A. Ferrone, Biophys. J. **46**, 631 (1984).
[28] F. A. Ferrone, J. Hofrichter, and W. A. Eaton, J. Mol. Biol. **183**, 591 (1985).
[29] F. A. Ferrone, J. Hofrichter, H. R. Sunshine, and W. A. Eaton, Biophys. J. **32**, 361 (1980).
[30] S. R. Collins, A. Douglass, R. D. Vale, and J. S. Weissman, PLoS Biol. **2**, e321 (2004).
[31] T. P. J. Knowles, C. A. Waudby, G. L. Devlin, S. I. A. Cohen, A. Aguzzi, M. Vendruscolo, E. M. Terentjev, M. E. Welland, and C. M. Dobson, Science **326**, 1533 (2009).
[32] S. I. A. Cohen, M. Vendruscolo, M. E. Welland, C. M. Dobson, E. M. Terentjev, and T. P. J. Knowles, J. Chem. Phys. **135**, 065105 (2011).
[33] T. C. T. Michaels, A. J. Dear, and T. P. J. Knowles, Phys. Rev. E **99**, 062415 (2019).
[34] A. J. Dear, G. Meisl, T. C. T. Michaels, M. R. Zimmermann, S. Linse, and T. P. J. Knowles, J. Chem. Phys. **152**, 045101 (2020).
[35] S. I. A. Cohen, S. Linse, L. M. Luheshi, E. Hellstrand, D. A. White, L. Rajah, D. E. Otzen, M. Vendruscolo, C. M. Dobson, and T. P. J. Knowles, Proc. Natl. Acad. Sci. U. S. A. **110**, 9758 (2013).
[36] G. Meisl, X. Yang, E. Hellstrand, B. Frohm, J. B. Kirkegaard, S. I. A. Cohen, C. M. Dobson, S. Linse, and T. P. J. Knowles, Proc. Natl. Acad. Sci. U. S. A. **111**, 9384 (2014).
[37] P. Flagmeier, G. Meisl, M. Vendruscolo, T. P. J. Knowles, C. M. Dobson, A. K. Buell, and C. Galvagnion, Proc. Natl. Acad. Sci. U. S. A. **113**, 10328 (2016).
[38] F. Kundel, L. Hong, B. Falcon, W. A. McEwan, T. C. T. Michaels, G. Meisl, N. Esteras, A. Y. Abramov, T. P. J. Knowles, M. Goedert, and D. Klenerman, ACS Chem. Neurosci. **9**, 1276 (2018).
[39] P. Arosio, M. Vendruscolo, C. M. Dobson, and T. P. J. Knowles, Trends Pharmacol. Sci. **35**, 127 (2014).
[40] S. I. A. Cohen, P. Arosio, J. Presto, F. R. Kurudenkandy, H. Biverstål, L. Dolfe, C. Dunning, X. Yang, B. Frohm, M. Vendruscolo, J. Johansson, C. M. Dobson, A. Fisahn, T. P. J. Knowles, and S. Linse, Nat. Struct. Mol. Biol. **22**, 207 (2015).
[41] P. Arosio, G. Meisl, M. Andreasen, and T. P. J. Knowles, Proc. Natl. Acad. Sci. U. S. A. **112**, 5267 (2015).
[42] P. Arosio, T. C. T. Michaels, S. Linse, C. Månsson, C. Emanuelsson, J. Presto, J. Johansson, M. Vendruscolo, C. M. Dobson, and T. P. J. Knowles, Nat. Commun. **7**, 10948 (2016).
[43] J. Habchi, P. Arosio, M. Perni, A. R. Costa, M. Yagi-Utsumi, P. Joshi, S. Chia, S. I. A. Cohen, M. B. D. Müller, S. Linse, E. A. A. Nollen, C. M. Dobson, T. P. J. Knowles, and M. Vendruscolo, Sci. Adv. **2**, e1501244 (2016).
[44] F. A. Aprile, P. Sormanni, M. Perni, P. Arosio, S. Linse, T. P. J. Knowles, C. M. Dobson, and M. Vendruscolo, Sci. Adv. **3**, e1700488 (2017).
[45] J. Habchi, S. Chia, R. Limbocker, B. Mannini, M. Ahn, M. Perni, O. Hansson, P. Arosio, J. R. Kumita, P. K. Challa, S. I. A. Cohen, S. Linse, C. M. Dobson, T. P. J. Knowles, and M. Vendruscolo, Proc. Natl. Acad. Sci, U. S. A. **114**, E200 (2017).
[46] S. Chia, J. Habchi, T. C. T. Michaels, S. I. A. Cohen, S. Linse, C. M. Dobson, T. P. J. Knowles, and M. Vendruscolo, Proc. Natl. Acad. Sci, U. S. A. **115**, 10245 (2018).
[47] A. E. Bryson, IEEE Control Syst. Mag. **16**, 26 (1996).
[48] G. W. Swan, Math. Biosci. **101**, 237 (1990).
[49] M. Engelhart, D. Lebiedz, and S. Sager, Math. Biosci. **229**, 123 (2011).
[50] H. Moore, J. Pharmacokinet. Pharmacodyn. **45**, 127 (2018).
[51] D. Kirschner, S. Lenhart, and S. Serbin, J. Math. Biol. **35**, 775 (1997).
[52] F. Chee, A. V. Savkin, T. L. Fernando, and S. Nahavandi, IEEE Trans. Biomed. Eng. **52**, 1625 (2005).
[53] T. C. T. Michaels, C. A. Weber, and L. Mahadevan, Proc. Natl. Acad. Sci. U. S. A. **116**, 14593 (2019).
[54] T. C. T. Michaels, A. J. Dear, J. B. Kirkegaard, K. L. Saar, D. A. Weitz, and T. P. J. Knowles, Phys. Rev. Lett. **116**, 258103 (2016).
[55] T. C. T. Michaels, A. J. Dear, and T. P. J. Knowles, New J. Phys. **20**, 055007 (2018).
[56] G. Meisl, J. B. Kirkegaard, P. Arosio, T. C. T. Michaels, M. Vendruscolo, C. M. Dobson, S. Linse, and T. P. J. Knowles, Nat. Protoc. **11**, 252 (2016).
[57] F. A. Ferrone, J. Hofrichter, and W. A. Eaton, J. Mol. Biol. **183**, 611 (1985).
[58] J. Hofrichter, J. Mol. Biol. **189**, 553 (1986).
[59] S. Campioni, G. Carret, S. Jordens, L. Nicoud, R. Mezzenga, and R. Riek, J. Am. Chem. Soc. **136**, 2866 (2014).
[60] C. L. L. Pham, A. Rey, V. Lo, M. Soulès, Q. Ren, G. Meisl, T. P. J. Knowles, A. H. Kwan, and M. Sunde, Sci. Rep. **6**, 25288 (2016).
[61] C. Galvagnion, A. K. Buell, G. Meisl, T. C. T. Michaels, M. Vendruscolo, T. P. J. Knowles, and C. M. Dobson, Nat. Chem. Biol. **11**, 229 (2015).
[62] J. Szavits-Nossan, K. Eden, R. J. Morris, C. E. MacPhee, M. R. Evans, and R. J. Allen, Phys. Rev. Lett. **113**, 098101 (2014).
[63] T. C. T. Michaels, A. J. Dear, and T. P. J. Knowles, Int. Rev. Phys. Chem. **35**, 679 (2016).
[64] G. McColl, B. R. Roberts, T. L. Pukala, V. B. Kenche, C. M. Roberts, C. D. Link, T. M. Ryan, C. L. Masters, K. J. Barnham, A. I. Bush, and R. A. Cherny, Mol. Neurodegener. **7**, 57 (2012).
[65] S. E. Schindler, J. G. Bollinger, V. Ovod, K. G. Mawuenyega, Y. Li, B. A. Gordon, D. M. Holtzman, J. C. Morris, T. L. Benzinger, C. Xiong, A. M. Fagan, and R. J. Bateman, Neurology **93**, e1647 (2019).
[66] L. C. Evans, An introduction to mathematical optimal control theory version 0.2, 1983, course notes; available at http://math.berkeley.edu/evans/control.course.pdf.
[67] A. Bensoussan, *Stochastic Control of Partially Observable Systems* (Cambridge University Press, 2004).

[68]R. Van Handel, Stochastic calculus, filtering, and stochastic control, 2007, course notes; available at http://www.princeton.edu/rvan/acm217/ACM217.pdf.
[69]R. E. Kalman, J. Basic Eng. **82**, 35 (1960).
[70]R. E. Kalman and R. S. Bucy, J. Basic Eng. **83**, 95 (1961).
[71]M. Athans and E. Tse, IEEE Trans. Autom. Control **12**, 690 (1967).
[72]T. Kailath, IEEE Trans. Autom. Control **13**, 646 (1968).
[73]Y. Bar-Shalom and E. Tse, IEEE Trans. Autom. Control **19**, 494 (1974).
[74]N. G. van Kampen, J. Stat. Phys. **24**, 175 (1981).